LINK RELATIONSHIP MEASUREMENTS IN LOAD-MODULATED UHF RFID

Daniel G. Kuester, David R. Novotny, and Jeffrey R. Guerrieri
National Institute of Standards and Technology
325 Broadway, Boulder, CO, 80304

ABSTRACT

This paper investigates the relative roles of the forward and reverse links in determining the operational range of passive UHF RFID systems. The relative importance of the links are discussed first in the free field as a first-order model. We then present measurements of boresight transmission and scattering off of a dipole in a somewhat reverberant storage room to investigate losses in the forward link compared to those in the reverse link with measurements similar to those in ISO 18047-6. Results normalized against semi-anechoic data showed disagreement between reverse link fading and the square of forward link fading by up to 8 dB within a measurement range of 2 m across 895-945 MHz.

1. Introduction

Successful object tracking in radio frequency identification (RFID) systems needs reliable radio links between readers and tags. Standardized test methods continue to evolve for characterizing reader and tag performance in these links, but the nature of passive load-modulated communication is physically different from better-established powered transmission systems, and less well understood.

This paper presents recent empirical work toward better understanding the fundamental behavior of the asymmetrical relationship between the forward (reader-to-tag) and load-modulated reverse (tag-to-reader) links. In the forward link of passive and active RFID systems, a reader transmits directly to its tag field, which receives data (and, in the passive case, its power supply) from the transmitted wave. In the reverse link, a tag varies its antenna load impedance encode information into modulated reflections from the same carrier from the reader. This link is physically different, because it is based on reflection and not transmission. Previous work can already explain the relationship between propagation losses in these links in the free field, but not in practical environments which impose multipath effects. This is in contrast with other systems which may use powered transmission in both link direction, where antenna reciprocity suggests propagation losses between antennas should be the same both ways [2].

Previous work has already considered link fading of passive UHF systems in realistic deployment environments. Forward link propagation models and simulations have been compared with experiment by many authors (e.g., [3]-[7]). These papers don't, however, address the fundamental relationship between multipath fading in these systems' forward and reverse links. If multipath were to effect the fading trends of the two links independently, then either might separately fade to the point of making communication impossible, representing a potential concern for system reliability.

Here, we discuss of the relationship between forward and reverse links in the free-field, and present S-parameter measurements which attempt to compare these links in a representative storage environment. The forward link losses are simulated by measuring $|S_{21}|$ between a commercial UHF patch antenna and a Roberts dipole tuned to 915 MHz. A reverse link is simulated by shorting the dipole and using it like the half-wavelength rod in ISO 18047-6, except phase is taken into account: a $|\Delta S_{11}|$ is reported as the difference between the reflection coefficient of the reader antenna with and without the shorted dipole in the test environment.

Table 1 – Link symbols in this paper

Continuous-wave power received at reader	$P_{rx}^{(cw)}$
Modulated power received at reader	$P_{rx}^{(mod)}$
Reader transmit power	P_{tx}
Power received at tag	P_{tag}
Reader, tag antenna isotropic gains	G_{rd}, G_{tag}
Wavelength, reader-tag separation	λ, R
Free-field forward, reverse link range	$R_{\rightarrow}, R_{\leftarrow}$
Threshold activation power density of tag	$W_{tag,th}$
Reader receive sensitivity threshold	$P_{rx,th}^{(mod)}$
Reader, tag impedance mismatch power losses	e_{rd}, e_{tag}
Polarization mismatch power loss	e_{pol}

2. Far-field system performance in free space

Variables used in this paper for far-field system performance are outlined in Table 1. For simplicity, dependence on signal parameters, doppler shift, and tag antenna detuning are neglected.

2.1. The forward link

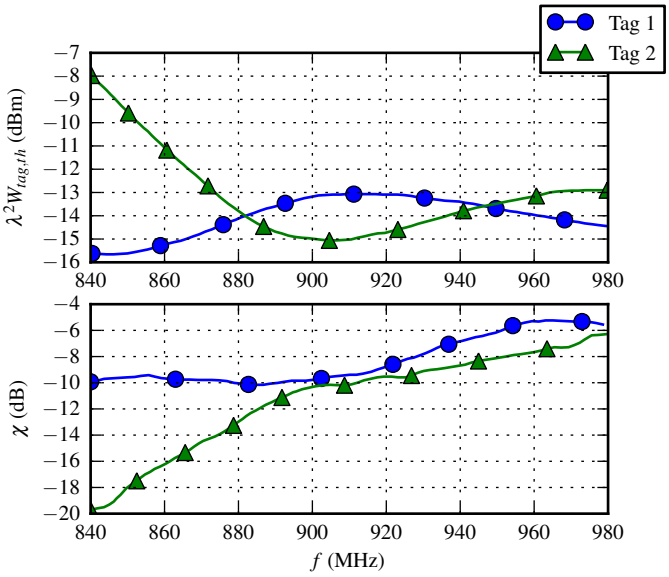

Figure 1 – Nikitin and Rao's characterization [9] of the sensitivity $\lambda^2 W_{tag,th}$ and backscattering factor χ of two commercially available tags. The tags were oriented broadside toward the reader antenna, and interrogated with the "case A" signal parameters.

A simple reader-to-tag transmission model is the far-field Friis transmission equation [2]

$$P_{tag} = P_{tx} G_{tag} G_{rd} e_{tag} e_{rd} e_{pol} \left(\frac{\lambda}{4\pi R}\right)^2, \tag{1}$$

where each variable except R depends on frequency. P_{tag}, e_{pol}, G_{tag}, and G_{rd} also vary with the antennas' relative orientation.

Power received by the tag must exceed a threshold $P_{tag,th}$ to turn on, corresponding to an incident power density of $W_{tag,th} = P_{tag,th}/(\lambda^2 G_{tag} e_{tag})$ [2]. An equivalent "tag sensitivity" that is often used in industry [9] is $\lambda^2 W_{tag,th}$. This threshold in terms of (1) is

$$P_{tx} G_{rd} e_{rd} e_{pol} \left(\frac{\lambda}{4\pi R}\right)^2 \geq \lambda^2 W_{tag,th}. \tag{2}$$

Because power delivered in this model decreases monotonically, a maximum forward link range $R_{\rightarrow}$ is

$$R_{\rightarrow} = \left(\frac{P_{tx}}{\lambda^2 W_{tag,th}} G_{rd} e_{rd} e_{pol}\right)^{1/2} \frac{\lambda}{4\pi}. \tag{3}$$

2.2. The reverse link

The scattered continuous-wave power $P_{rx}^{(cw)}$ received at the reader from an object with a radar cross-section σ can be estimated in the far field with the monostatic radar equation [2]:

$$P_{rx}^{(cw)} = P_{tx} (G_{rd} e_{rd} e_{pol})^2 \frac{\lambda^2}{(4\pi)^3 R^4} \sigma. \tag{4}$$

If the target is a tag modulating its antenna load impedance between two states creating a modulated "delta" or "differential" radar cross-section" $\Delta\sigma$, then a corresponding modulated power received at the reader $P_{rx}^{(mod)}$ is

$$P_{rx}^{(mod)} = P_{tx} (G_{rd} e_{rd} e_{pol})^2 \frac{\lambda^2}{(4\pi)^3 R^4} \Delta\sigma. \tag{5}$$

A convenient and equivalent expression for link calculations uses a "tag scattering loss" defined as $\chi = 4\pi\Delta\sigma/\lambda^2$ so that

$$P_{rx}^{(mod)} = P_{tx} (G_{rd} e_{rd} e_{pol})^2 \left(\frac{\lambda}{4\pi R}\right)^4 \chi. \tag{6}$$

Both $\Delta\sigma$ and χ depend not only on relative polarization, tag orientation, and frequency like $W_{tag,th}$, but also power incident on the tag [10].

If the reader's receive sensitivity is $P_{rd,th}^{(mod)}$, then the reverse link must satisfy

$$P_{tx} (G_{rd} e_{tx} e_{pol})^2 \left(\frac{\lambda}{4\pi R}\right)^4 \chi \geq P_{rx,th}^{(mod)} \tag{7}$$

for a successful link. The maximum reverse-link range $R_{\leftarrow}$ is therefore

$$R_{\leftarrow} = \left[\frac{P_{tx}\chi}{P_{rx,th}^{(mod)}}\right]^{1/4} (G_{rd} e_{rd} e_{pol})^{1/2} \frac{\lambda}{4\pi} \tag{8}$$

in free space.

2.3. System performance

Examples of recent tags' $W_{tag,th}$ and χ measured by Nikitin and Rao [9] are shown in Fig. 1. Free-field read range estimates from (3) and (8) with a reader radiating $P_{tx} = 28$ dBm are shown in Fig. 2.

The assumption (as in [3]-[7]) that the overall system read range is limited by $R_{\rightarrow}$ can be checked by comparing it against $R_{\leftarrow}$. A figure of merit can be defined as the ratio of (3) and (8):

$$\frac{R_{\rightarrow}}{R_{\leftarrow}} = \left[\frac{P_{tx} P_{rd,th}^{(mod)}}{\chi (\lambda^2 W_{tag,th})^2}\right]^{1/4}, \tag{9}$$

which is less than one if the forward link is the main constraint. Interestingly, this quantity is independent of antenna properties for monostatic systems.

Values of $R_{\rightarrow}/R_{\leftarrow}$ from Fig. 2 at 915 MHz are shown in Table 2. Note that the forward link is only the constraining link in this free-field model if the reader's receive sensitivity is below -66 dBm. If tag sensitivities continue to improve, then (9) suggests the reverse link will become a more important constraint.

3. Link performance with multipath

This section presents measured UHF scattering and transmission behavior in both a semi-anechoic environment and a more reverberant indoor storage environment to investigate multipath fading performance.

3.1. Measurement technique

To reduce measurement complexity from RFID protocol signaling, measurements were performed with a network analyzer. These signals were assumed to be similar enough to UHF RFID systems' narrowband signaling to exhibit the same propagation behavior. Two commercial 902-928 MHz 8 dBi RFID reader antennas were chosen: one linear polarized (LP), and the other circular polarized (CP). A Roberts dipole [11] tuned to 915 MHz was chosen as the "tag" target to resemble dipole-based designs used in common tags. The antennas' matching performance are plotted in Fig. 4.

Measurements were performed in each configuration shown in Fig. 3. First, a transmission measurement is per-

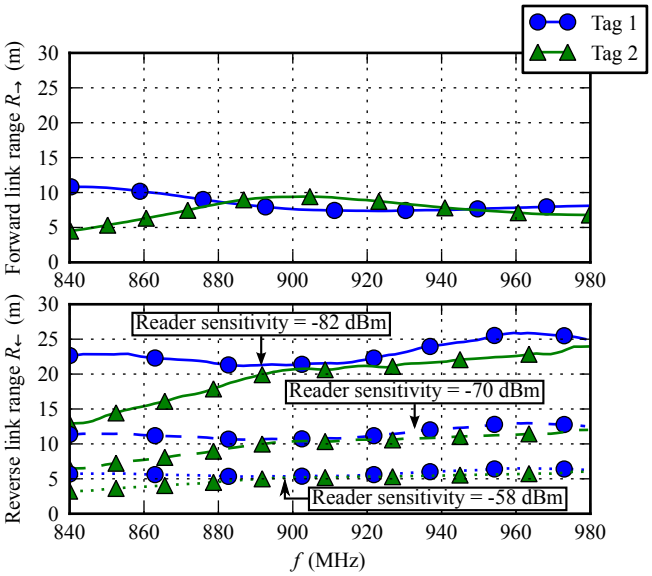

Figure 2 – System range estimates of the tags in Fig. 1 positioned the far field and free space. The estimates use (3) and (8), with $P_{tx} = 28$ dBm, matched impedances and polarizations, and $G_{rd} = 8$ dBi. The reverse link is shown with some example reader sensitivities $P_{rd,th}^{(mod)}$.

Table 2 – Free-field relative link range figures of merit $R_{\rightarrow}/R_{\leftarrow}$ near 915 MHz for example reader sensitivities, taken from fig. 2.

$P_{rd,th}^{(mod)}$	$R_{\rightarrow}/R_{\leftarrow}$	Weakest link
-58 dBm	1.6	Reverse
-70 dBm	0.8	Forward
-82 dBm	0.4	Forward

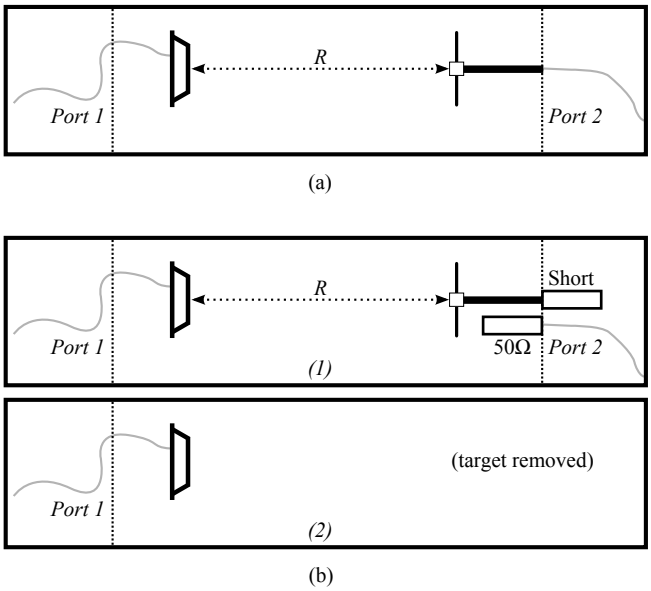

Figure 3 – Measurement setup. In (a) the forward link configuration, a $|S_{21}|^2$ measurement was performed with the network analyzer, calibrated to S-parameter planes at ports 1 and 2. For (b) the reverse link, measurements of the reflection coefficients at port 1 were measured (1) with the dipole shorted without moving it from (a), then (2) with the dipole removed from the environment. The magnitude of the difference $|\Delta S_{11}|$ was taken as the received modulation signal.

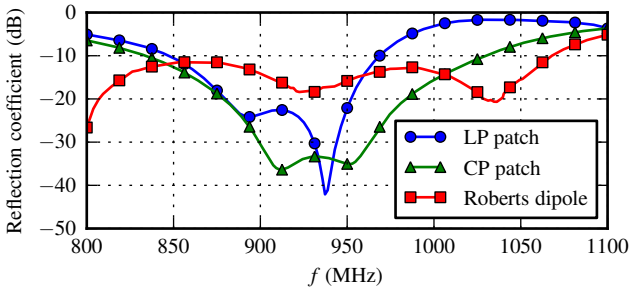

Figure 4 – Reflection coefficients of the three antennas under test. The two patches are commercially available RFID reader patch antennas. The dipole resembles common tag antenna types.

Table 3 – Regression information from Fig. 6, 895-935 MHz

	$\lvert S_{21}\rvert$ *Std. dev.*	$\lvert\Delta S_{11}\rvert$ *Std. dev.*	*Apparent phase center offset*
CP patch	0.05 dB	0.22 dB	0.008 - 0.049 m
LP patch	0.07 dB	0.45 dB	0.042 - 0.059 m

formed to imitate a passive RFID forward link, with S-parameters calibrated as shown in Fig. 3a; the recorded value is $|S_{21}|^2 = P_{tag}/P_{tx}$ (the value modeled in (1) for the free-field case). Figure 3b shows the procedure used to measure the difference detected between tag backscattering states in a reverse link. This is the same approach used for the cross-section measurement calibration outlined in ISO/IEC 18047-6, with the $\lambda/2$ Roberts dipole shorted (and leaving its feed cable with a matched termination) instead of a $\lambda/2$ rod. The reflection coefficient at one of the "reader" patch antennas is measured in each of the two states of the "tag" simulated in Fig. 3b: the test environment (1) with, then (2) without the shorted dipole and matched feed. The magnitude of the difference between the two values is reported, so that $|\Delta S_{11}|^2 = P_{rx}^{(mod)}/P_{tx}$. The noise floor of $|\Delta S_{11}|$ was below -75 dB across 700-1100 MHz.

Measurements were taken in the semi-anechoic and storage environments shown in Fig. 5. For each set of transmission and scattering measurements, both the patch and dipole antennas were aligned to boresight orientation with a laser square, and co-polarized with a level. This procedure was repeated in each environment and for each reader antenna. The range R between the two antennas (shown dotted in Fig. 3) was measured by laser range finder in each experiment.

3.2. Measurement results

Measurements of scattering and throughput in the semi-anechoic chamber $|\Delta S_{11}^{(an)}|$ and $|S_{21}^{(an)}|$ are plotted against range R in Fig. 6 at 902 MHz and 928 MHz. Regressions to $1/R^2$ and $1/R^4$ accounting for apparent phase centers are shown to validate the anechoic performance of the chamber; some information about the regression fit quality and apparent phase centers are shown in Table 3.

To make multipath effects clear, results from the storage room environment are normalized to semi-anechoic chamber data in Fig. 7 by means of (10) and (11):

Figure 5 – The semi-anechoic chamber (left) and storage room (right) test environments. The LP reader antenna is shown in each on its steel mounting structure, boresight to the dipole target.

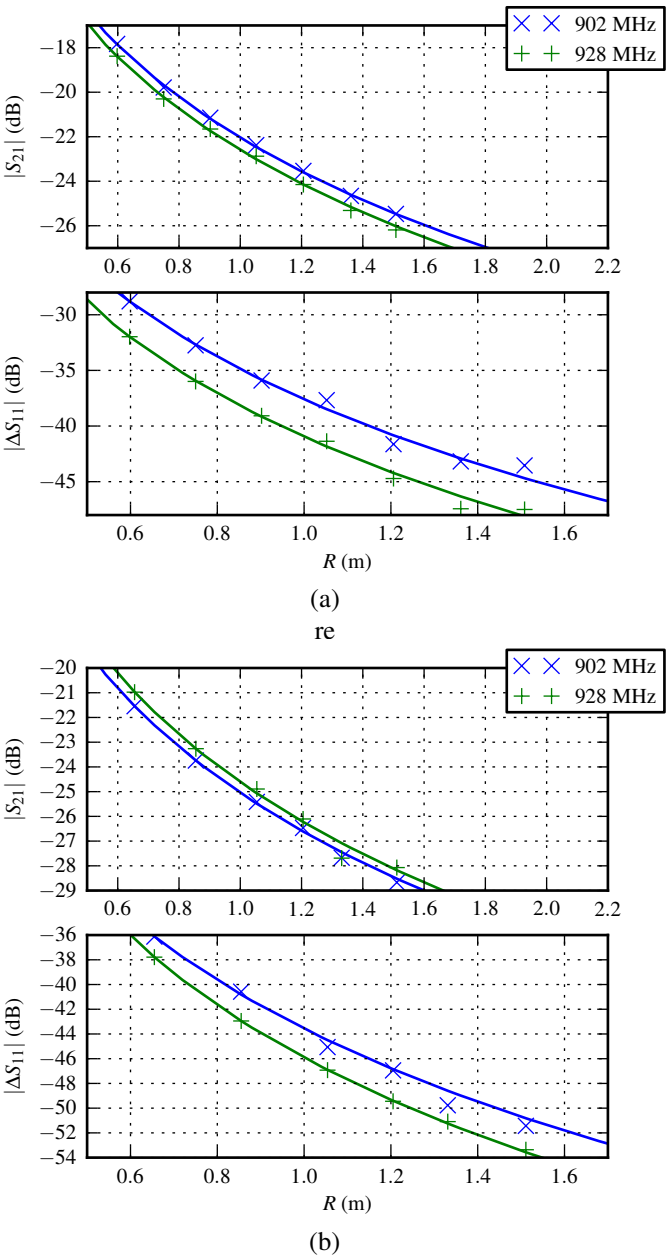

Figure 6 – Throughput and scattering measurements against range with (a) the 8 dBi LP patch and (b) the 8 dBi CP patch antennas. The curves are fitted to R dependences as appropriate in (2) and (6), and to apparent phase centers. Regression information across 895-935 MHz are in Table 3.

Table 4 – Combined uncertainty estimates of random alignment errors and noise at 915 MHz with coverage factor 2.

Measurement	Uncertainty estimate
$\lvert S_{21}\rvert^2$	0.2 dB (at worst case, $R = 0.6$ m)
$\lvert \Delta S_{11}\rvert^2$	0.9 dB (at worst case, $R = 2$ m)
$F_{\rightarrow}$	0.3 dB
$F_{\leftarrow}$	1.2 dB
$F_{\rightarrow}^2/F_{\leftarrow}$	1.3 dB

$$F_{\rightarrow} = \frac{|S_{21}|^2}{|S_{21}^{(an)}|^2} \tag{10}$$

for the forward link, and

$$F_{\leftarrow} = \frac{|\Delta S_{11}|^2}{|\Delta S_{11}^{(an)}|^2} \tag{11}$$

in the reverse link. $|S_{21}|^2$ and $|\Delta S_{11}|^2$ are measured in the fading test environment (the storage room) the same way as for the semi-anechoic cases.

Figure 7 shows $F_{\rightarrow}$ and $F_{\leftarrow}$ at various distances between the reader antennas and the dipole target in the storage environment shown in Fig. 5b. Corresponding uncertainty estimates are shown in Table 4. As R increases, multipath effects tend to become more significant in both links.

Notably, the $F_{\rightarrow}$ and $F_{\leftarrow}$ curves show similar contours, but simply squaring the one-way fading ($F_{\rightarrow}^2$) does not match the reverse link fading $F_{\leftarrow}$. Across all measurements within 895 - 935 MHz, that discrepancy $F_{\rightarrow}^2/F_{\leftarrow}$ (plotted in Fig. 8) ranged from -6 to +8 dB, which is beyond the 1.3 dB uncertainty estimate.

4. Conclusion

We have demonstrated here empirically that multipath fading effects in modulated scattering links may not exhibit a clear relationship with transmission links, when the reverse link is measured as in ISO 18047-6. Even within a relatively close 2 m reader to tag range, the forward link transmission fading squared differed from the scattered fading by up to 8 dB. Future work will continue to investigate measurement and test methods to better understand this relationship.

5. Acknowledgements

The author thanks Pavel Nikitin for his data, and Randal Direen for his help constructing the anechoic range.

The Department of Homeland Security Science and Technology Directorate has, in part, sponsored the production of this material with NIST.

References

[1] D.R. Novotny, J.R. Guerrieri, D.G. Kuester, "Potential interference issues between FCC part 15 compliant UHF ISM emitters and equipment passing standard immunity testing requirements," *Proc. 2009 Symp. on Electromagnetic Compatibility*, pp.161-165, 17-21 Aug. 2009.

[2] C.A. Balanis, *Antenna Theory: Analysis and design, 3rd ed*. Hoboken, NJ: Wiley & Sons, 2005, pp. 94-99.

[3] L.W. Mayer, M. Wulich, S. Caban, "Measurements and channel modeling for short range indoor UHF applications," *Proc. 2006 European Conf. on Antennas and Propagation*, pp.1-5, 6-10 Nov. 2006.

[4] H.G. Wang , C.X. Pei, C.H. Zhu, "A link analysis for passive UHF RFID system in LOS indoor environment," *Proc. 4th Intl. Conf. on Wireless Communications, Networking and Mobile Computing (WiCOM)*, pp. 1-7, 2008.

[5] K.Y. Jeon, S.H. Cho, "Performance of RFID EPC C1 Gen2 Anti-collision in multipath Fading Environments," *Proc. 2nd Intl. Conf. on Communication Theory, Reliability, and Quality of Service*, pp. 20-25, Jul. 2009.

[6] W. Su, K.M. Beilke, T.T. Ha, "A reliability study of RFID technology in a fading channel," *Proc. Asilomar Conf. on Signals, Systems, and Computers*, pp. 2124-2127, 4-7 Nov. 2007.

[7] J.-W. Jung, J-H. Hwang, Y.-J. Moon, H.-K. Kwak, H.-H. Roh, J.-S. Park, M.-S. Kang, "Multipath fading measurement on the circularly propagated UHF RFID reader antennas in a practical area", *Proc. Asia-Pacific Symposium on Electromagnetic Compatibility*, pp. 315-318, 19-23 May 2008.

[8] *Radio frequency identification device conformance test methods — Test methods for air interface communications at 860 MHz to 960 MHz*, ISO/IEC standard 18047-6, 2006.

[9] P.V. Nikitin and K.V.S. Rao, "Effect of gen2 protocol parameters on RFID tag performance," *Proc. 2009 Intl. Conf. on RFID*, pp.117-122, 28-29 Apr. 2009.

[10] S. Skali, C. Chantepy, S. Tedjini, "on the measurement of the delta radar cross section (ΔRCS) for UHF tags," *Proc. 2009 Intl. Conf. on RFID*, pp.346-351, 28-29 Apr. 2009.

[11] D. Morgan, *A handbook for EMC testing and measurement*. Institution Of Engineering And Technology, 1994, pp. 92-93.

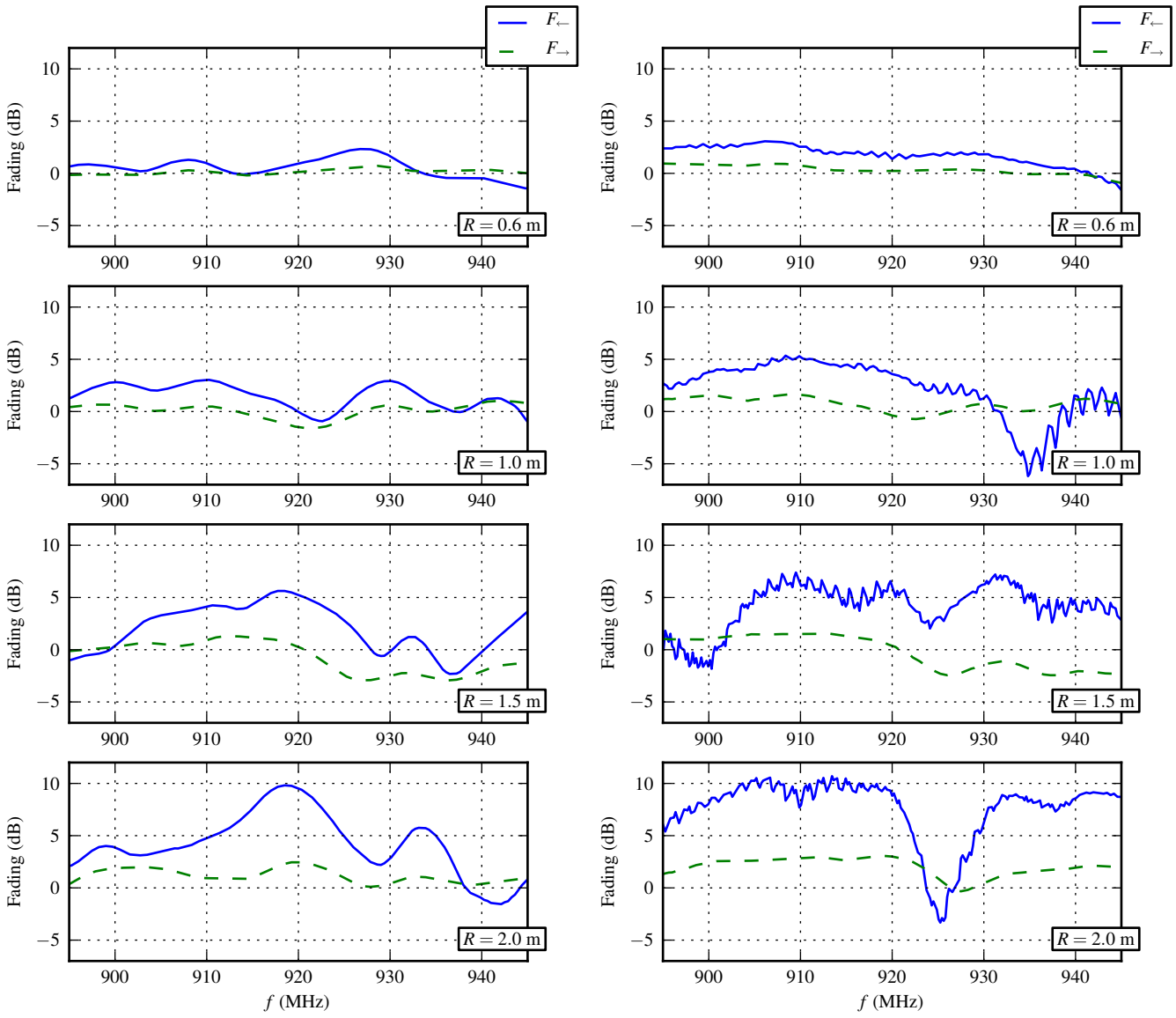

Figure 7 – Multipath fading with the (a) LP and (b) CP patch antennas. The curves show measurements from the reverberant environment (shown in Fig. 5)b normalized to the regressions in Fig. 6. Peaks and nulls tend deeper as the separation R between the reader antenna and the target increases.

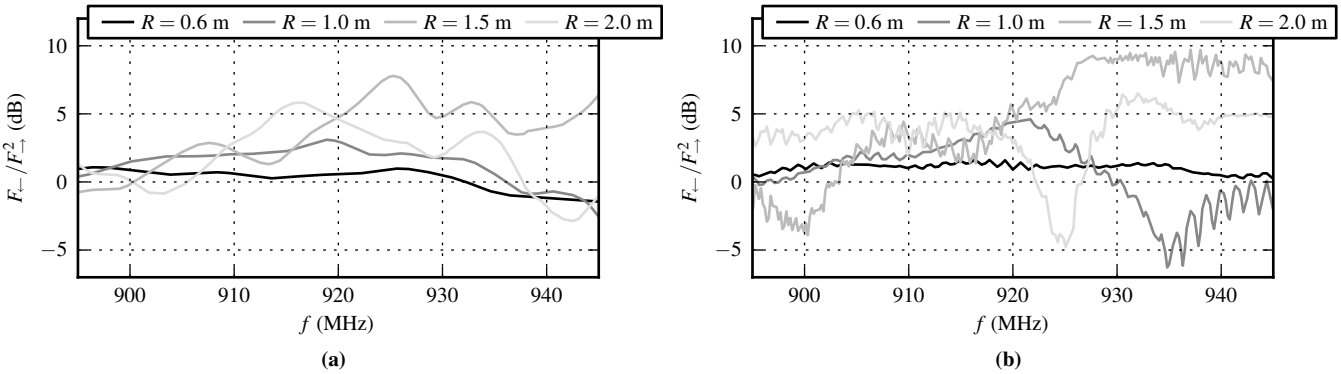

Figure 8 – The discrepancy $F_{\leftarrow}/F_{\rightarrow}^2$ between forward and reverse link fading from measurements taken with the (a) LP and (b) CP patch antennas, computed with the data in Fig. 7. The random uncertainty here is estimated to be 1.3dB (Table 4).